ELSEVIER

Cement & Concrete Composites 23 (2001) 345–352

Cement & Concrete Composites

www.elsevier.com/locate/cemconcomp

Microcracking and strength development of alkali activated slag concrete

Frank Collins [a,*], J.G. Sanjayan [b]

[a] Maunsell Pty Ltd, Level 9, 161 Collins Street, Melbourne, Victoria 3000, Australia
[b] Department of Civil Engineering, Monash University, Clayton, Victoria 3800, Australia

Received 23 August 2000; accepted 3 January 2001

Abstract

Alkali activated slag concrete (AASC) is made by activating ground granulated blast furnace slag with alkalis without the use of any Portland cement. This study investigates the level of microcracking which occurs in AASC when subjected to various types of curing regimes. The corresponding compressive strength developments of AASC were monitored. The level of microcracking were measured using three different types of tests: (1) frequency and size of surface cracks using crack-detection microscope (2) water sorptivity tests measuring absorption of water by capillary attraction and (3) mercury intrusion porosimetry (MIP) tests which measured the pore size distribution of AASC and AAS pastes (AASPs). The results show that the lack of moist curing of AASC increased the level of microcracking measured using all three different tests mentioned above. The strength development of AASC is also significantly reduced by lack of moist curing.

Keywords: Strength development; Microcracking; AASC; AASPs

1. Introduction

Alkali activated slag concrete (AASC) is made with 100% ground granulated blast furnace slag activated by alkalis, instead of the Portland cement in the binder of concrete. Details of AASC can be found in [33].

AASC shares the same sensitivity to lack of curing found in concretes made with slag blended cements (blend of Portland cement and slag). Wainwright [34], Butler and Ashby [3], and Butler and Ashby [4] found high sensitivity of slag blended cement concrete to lack of moist curing and found significantly lower compressive strength than companion samples cured in lime saturated bath water. Swamy and Bouikni [31] showed that concrete mixtures containing 65% slag as the cementitious binder have strength retrogression when air cured. Nakamura et al. [24] measured up to 30–40% lower compressive strength of air cured 50% slag blended cement concrete compared with bath cured concrete. However, Wainwright [34] argues that this may be a size effect since the strength loss in larger samples is not as pronounced. In the case of 40 MPa concrete with 50% slag blended cement as the binder, Sioulas [30] measured 17% lower compressive strength of sealed cured cylinders compared with bath cured cylinders. Furthermore, Sioulas [30] showed the cores taken from large columns made of blended cement concrete (up to 70% replacement of Portland cement with slag) had up to 35% less strength than the bath cured cylinder strength, and had significantly less strength than that of companion ordinary Portland cement (OPC) concrete columns.

The strength of AASC is also sensitive to the relative humidity (RH) of the curing environment. Talling and Brandstetr [33] report that loss of moisture during dry air storage reduces strength between 7 and 28 days, however the magnitude of strength loss and the type of activator is unreported.

Slag binder that has been activated by NaOH shows lower strength following exposed curing. Kutti and Malinowski [18] showed there is considerable decrease in compressive strength when comparing air-dried NaOH alkali activated slag mortar (AASM) at 50% RH and 20°C with bath cured NaOH AASM samples at 20°C. Byfors et al. [5] measured up to 20% lower compressive strength when comparing water cured AASC

* Corresponding author. Tel.: +61-3-9653-1234; fax: +61-3-9654-7117.
E-mail address: fgco@maunsell.com.au (F. Collins).

0958-9465/01/$ - see front matter
PII: S0958-9465(01)00003-8

with air cured (50% RH) AASC after initial seven days wet curing. Kukko and Mannonen [17] measured lower early age compressive strength when comparing samples cured at 40% RH and 20°C) with samples cured at 95% RH and 20°C, however, following one year, the compressive strength was almost identical. Kutti et al. [19] measured 35% lower compressive strength between NaOH activated AASM cured at 33% RH and 20°C at 36 months and companion samples cured at 94% RH 20°C. However, when exposed at RH of 76% and 86%, the samples show similar compressive strength to prisms cured at 94% RH. Hakkinen [13] showed that NaOH activated AASC cylinders moist cured for seven days followed by exposure to 40% RH and 20°C were 10.5% lower in compressive strength at one year compared with companion samples cured at 70% RH and 20°C.

For sodium silicate AASM, Anderson and Gram [1] measured lower compressive strength of air cured (80% RH and 20°) AASM compared with ordinary Portland cement mortar (OPCM) up to seven days. However, beyond seven days AASM showed better compressive strength than OPCM. Following air storage at 95% and 70% RH and 20°C, Talling [32] reports little difference in cylinder strength of sodium silicate activated AASC. However, when stored at 50% RH and 20°C, strength development stops after 28 days and the strength at 91 days is 14% lower than companion samples stored at 95% RH.

Hakkinen [13] showed that dry exposed NaOH activated AASC displays a size effect, whereby the strength of 150-mm diameter cylinders is less affected than 100-mm diameter cylinders by microcracks developed during drying. However, the strength variations of a sample thicker than 150 mm following exposed curing is unreported.

This paper describes the effect of microcracking on the strength development of AASC cylinders subjected to different curing types.

2. Experimental programme

2.1. Constituent materials and concrete and paste mixtures

The chemical composition and properties of the slag is summarised in Table 1. The term water/binder (w/b) ratio is used instead of the conventional water/cement ratio to describe the non-Portland cement binder. The slag is supplied with gypsum (2% SO_3) which is blended with the slag. The dry powdered sodium silicate activator (composed of 29% Na_2O, 28% SiO_2, and 43% H_2O) was pre-blended with the slag in the dry form prior to use for concrete manufacture. The hydrated lime activator (1% lime in water slurry form) was added to the mix with the mixing water.

Table 1
Properties of cementitious materials

Constituent/property	Slag
SiO_2 (%)	35.04
Al_2O_3 (%)	13.91
Fe_2O_3 (%)	0.29
MgO (%)	6.13
CaO (%)	39.43
Na_2O (%)	0.34
TiO_2 (%)	0.42
K_2O (%)	0.39
P_2O_5 (%)	<0.1
MnO (%)	0.43
Total sulphur as SO_3 (%)	2.43
Sulphide sulphur as S^{2-}	0.44
Cl (ppm)	80
Fineness (m^2/kg)	460
Loss on ignition (%)	1.45

The coarse aggregate consisted of 14 mm maximum size basalt with a specific gravity of 2.95 and 24 h water absorption of 1.2%. The fine aggregate consisted of river sand with a specific gravity of 2.65, 24 h water absorption of 0.5%, and a fineness modulus of 2.19.

The concrete mixture proportions are summarised in Table 2. The materials used for concrete making and the method of preparing concrete mixes in the laboratory were in accordance with Australian Standards. Collins and Sanjayan [8] have previously reported the fresh and mechanical properties of the concrete mix shown in Table 2.

Paste mixtures were also made to investigate the pore size distribution by mercury intrusion porosimetry (MIP). Mixing of AAS paste (AASP) was conducted in a 20-l stainless steel mixing bowl. Mixing was by machine at 98 revolutions per minute in a *Kenwood KNM20* planetary mixer. The slag and sodium silicate activator was pre-blended in the dry form for 2 min. The mixing water was then added. The hydrated lime was added as a

Table 2
Summary of concrete mixture proportions (kg/m^3)

Constituents	AASC[a]
Slag	360
Free water[b]	180
w/b	0.5
Fine aggregate	830
Coarse aggregate 14 mm	1130
Air content %	1.2

[a] Slag activated by powdered sodium silicate and lime slurry.
[b] Adjustments made for water in aggregates (to saturated surface dry condition), lime slurry, and sodium silicate.

1:3 hydrated lime: water slurry. The mixing procedure was 2-min mixing followed by 2 min of rest, followed by further mixing for 2 min. The fluid pastes were poured into cylindrical moulds, which had internal dimensions 63 mm diameter × 98 mm length. The w/b of AASP was 0.5. Following demoulding at one day, samples from each paste type were exposed to 23°C and 50% RH for 3, 7, 28, and 56 days. At the required time of test, the samples were crushed to a size adequate to pass a 2.36-mm sieve.

2.2. Compressive strength tests

Standard cylinders (100 mm diameter and 200 mm height) were made in accordance with Australian Standard AS1012, Parts 8 and 9 for compressive strength testing. Following demoulding, the cylinders were subjected to one of three curing regimes: *bath*, *exposed* or *sealed*. The definitions of the curing regimes are:

1. bath – immersed in saturated lime water at 23°C;
2. sealed – specimen is storage in two polythene bags and a sealed container so that no moisture movement in or out of the specimen. The specimen temperature was maintained at 23°C;
3. exposed – air exposed at 50% RH and 23°C.

The cylinder specimens were tested under compression in triplicate at 1, 3, 7, 28, 56, 91, 365 days.

Following compressive strength testing of AASC at 365 days, fragments of a size adequate to pass a 2.36-mm sieve were obtained from the concrete test cylinders for subsequent MIPs testing.

2.3. Surface crack measurements

For each cylinder, a line parallel to the longitudinal axis of the cylinder was drawn at the third points around the circumference. At the central 100 mm length of each of these three lines, the number of cracks and crack size was measured. The crack width was measured with a crack-detection microscope that had a 4-mm range, 0.01-mm divisions, 40× magnification, and built-in light source.

2.4. MIP tests

The pore size distribution was determined using a Micromeritics Autopore III 9429 porosimeter which was capable of pressures from 0 to 414 MPa (60,000 psi). A hydraulic pump generates the pressure and a contact sensor measures the mercury volume. All operations are automated by microprocessor and are conducted within a fully enclosed pressure chamber. The assumed surface tension of the triple-distilled mercury was 0.484 N/m at 25°C (ASTM D 440484 1992). The density of the mercury was 13.546 g/ml and the assumed contact angle was 140°.

2.5. Water sorptivity tests

The MIP results only provide data on very small-scale samples and therefore the extent of microcracking across a larger cross-sectional area of concrete was examined by water sorptivity testing. Therefore water sorptivity testing of the 100-mm diameter test cylinders was conducted to determine whether microcracking causes significant connected voids, thus leading to reduced compressive strength of AASC during exposed curing.

Additional cylinders that were exposed to bath, sealed, and exposed curing for 1, 3, 7, 28, and 56 days were saw cut into two halves. The purpose of saw cutting is to eliminate skin effects at the top or bottom concrete surface. One half of each cylinder was tested for water sorptivity, based on the procedure of Bamforth et al. [2].

The water sorptivity test measures capillary effects when one face of the sample is just in contact with water. The uptake of water, registered as vertical height rise and weight gain, is determined over a period of time. The capillary pores in concrete cause absorption of water by capillary attraction. Hence, a measure of the rate of absorption provides a useful indication of the pore continuity of the concrete. The technique of Bamforth et al. [2] relies on a simple set-up where one face of the sample is immersed to a depth of 1–2 mm and the weight gain and height rise of the sample is monitored with time. In unsaturated concrete, water absorption is linearly related to the square root of time, with the slope of the line defining sorptivity of the material.

3. Compressive strength development

Compressive strength development of the standard cylinders subject to bath, sealed, and exposed curing is shown in Fig. 1. Fig. 1 shows that the strength of sealed cured cylinders is lower than bath cured; after 365 days the strength difference is 21%. The sealed cured cylinders show little strength gain between 91 days and 1 yr. Fig. 1 shows 17% strength loss of exposed cylinders between 56 and 365 days. The strength of the exposed cylinders is 54% and 41% less than bath and sealed cylinders strengths, respectively, at 365 days. Strength retrogression of AASC cylinders subjected to exposed curing has not been reported previously in the literature.

4. Surface microcracking

AASC cylinders that were exposed to 23°C and 50% RH from Day 1 onwards developed visible surface

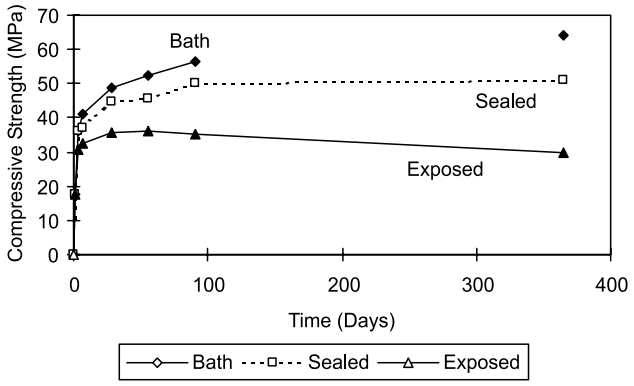

Fig. 1. Effect of type of curing on compressive strength, AASC, $w/b = 0.5$.

crazing cracks, or microcracking (Fig. 2). The cause of microcracking may be due to the very dry condition of the surface concrete, as evidenced by zero measured bleed [8], and also restraint of shrinkage-prone AASP by rigid basalt coarse aggregate. The cylinders that were cured under sealed and bath conditions showed no visible surface microcracking.

The crack frequency (number of cracks per sample) for at 3, 7, 28, and 56 days is summarised in Fig. 3.

The results show that the majority of microcracks occur within the first three days and are mostly of the size 0.01 mm. The frequency of the 0.01-mm crack size reaches a maximum at 7 days followed by crack width growth. The widths of the microcracks are as high as 0.3 mm.

Hsu et al. [15] showed that microcracks exist at the interface between coarse aggregate and mortar before any load is imposed, and the microcracks are caused by mortar volume changes. AASC shows significantly greater shrinkage strains than OPCC when subjected to drying conditions [8] and it is likely that the restraint provided by the stiff basalt coarse aggregate and the high shrinkage of the AASP has lead to microcracking under drying conditions. Meyers et al. [23] and Ravindrarajah and Swamy [25] have shown that the microcrack density increases with the magnitude of drying shrinkage. High shrinkage of the paste can lead to interconnected microcracks, as shown by Sicard et al. [29], in the case of very high strength concrete, due to desiccation. In the case of repairs to reinforcement corrosion damaged concrete, Collins and Roper [7] showed that the depth of the zone of microcracking, observed near the repair mortar to concrete substrate interface, had a strong influence on the soundness of the repair. Carrasquillo et al. [6] asserts that the development of combined microcracks is an essential step in the progression toward impending failure.

Following microscopic examination, Malolepszy and Deja [21] observed negligible microcracks on 7-day water cured AASM, however, when the same samples were subsequently exposed to 65% RH and 20°C, microcracking was observed. Byfors et al. [5] also observed microcracking on AASC and, following microscopic examination, concluded that the frequency was greater following exposed curing and this lead to reduced flexural strength. Cracking is more frequent and intense for concrete with binders composed of alkali activated slag than OPC and slag blended cements [11] and with increased activator content [12]. At low aggregate/cement ratio the microcracks become long and continuous [10]. Kutti and Malinowski [18] and Kutti et al. [19] conclude that the microcracking is due to the formation of an unstable (during drying) gel phase within the activated slag paste. During drying, a number of breaks in the particle to particle bonds throughout the gel structure occur thereby forming microcracks in the paste. Hakkinen [14] showed that microcracking is most pronounced within the zone of drying and that 150-mm diameter cylinders, which have a smaller proportion of the cross-section affected by surface drying and hence

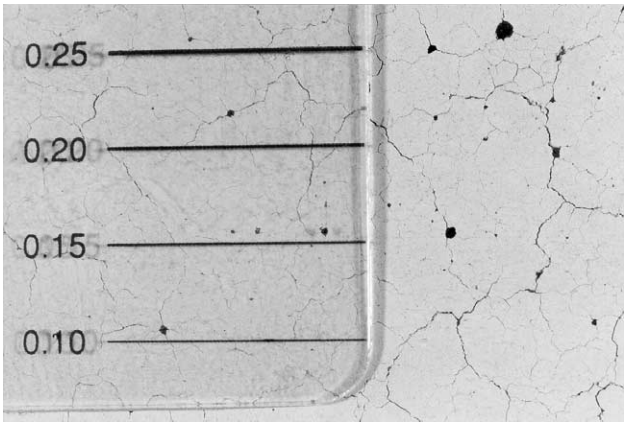

Fig. 2. Microcracks on AASC exposed to 50% RH and 23°C from Day 1 onwards.

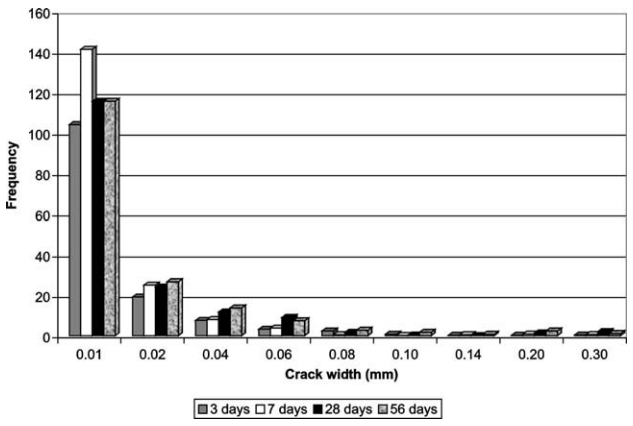

Fig. 3. Microcrack frequency of AASC exposed to 50% RH and 23°C from Day 1 onwards.

microcracking, show greater compressive strength than 100-mm diameter cylinders.

5. Pore size distribution

It is well established that blended slag cement binders have a finer pore size distribution than OPC binders [9,22,27,20,26,28,35].

AAS is sensitive to the type of curing. When subjected to air curing, however, alkali activated slag binder has higher number of pores in the 100–10,000 nm range than OPC binder [1,10,12,13]. Hakkinen et al. [10] showed that as hydration proceeds, under drying conditions, activated slag binder has an increasing number of pores within the 1000–10000 nm range, whereas the number of pores for OPC binder remains constant. The cause of increasing porosity within the 1000–10000 nm range is microcrack development [12,13].

Fig. 4 shows the cumulative pore size distributions for bath cured AASP with $w/b = 0.5$. At one day, the pore size distribution of AASP is coarse. From 1 to 3 days, there is a significant shift towards a finer pore size distribution. The results show increasing pore refinement with increasing age.

Fig. 5 shows the cumulative pore size distributions for sealed cured AASP with w/b 0.5. The pore size distributions are very similar to the bath cured results shown in Fig. 4.

The bath and sealed paste samples that were under test were taken from the centre (interior) of the sample. However, microcracking was visible on the surface of the exposed AASP samples and therefore MIPS testing was also undertaken at the outside and midway between the centre and outside of the sample. Fig. 6 shows cumulative pore size distribution of exposed AASP at 3, 7, 28, and 56 days.

Fig. 6 shows significantly coarser pore size distribution at the exterior and interior locations than bath and sealed cured specimens shown in Figs. 4 and 5, demonstrating the effects of lack of curing. The pore size distribution becomes coarser with distance towards the exterior of the sample, however the total porosity at 3, 7, and 28 days is very similar for all sample locations. At 56 days, the exterior pore size distribution is significantly coarser and the total porosity higher than at the internal sample location and this is reflected by cessation of growth of compressive strength for concrete tested at the same age.

Table 3 shows the proportion of pores within the mesopore, macropore, and voids/microcracks for AASP, based on the IUPAC [16]. There is a higher proportion of pores within the voids/microcracks pore size region up to 28 days. Many of the microcracks that were identified and discussed above are too large to be measured by MIPS and hence are not shown in Table 3.

Samples of 365 day AASC from standard cylinders that were subjected to bath, sealed, and exposed curing were tested by MIPS and the cumulative pore size distribution for concrete subjected to each of the curing types is shown in Fig. 7.

The pore size distributions of bath and sealed cured AASC are almost identical. This is despite the differences that were measured in compressive strength. Exposed AASC has considerably coarser pore size distribution than both bath and sealed cured AASC. For the exposed sample taken from the interior of the cylinder, the total porosity is almost the same as the bath and sealed cured samples. However, in the case of the exposed sample taken from the exterior, the total porosity is 3.67% greater than the sample taken from the interior of the exposed cylinder. Although there is likely to be errors introduced by aggregate contamination in the sample, the effect of microcracking on the pore size distribution is evident in the exposed samples.

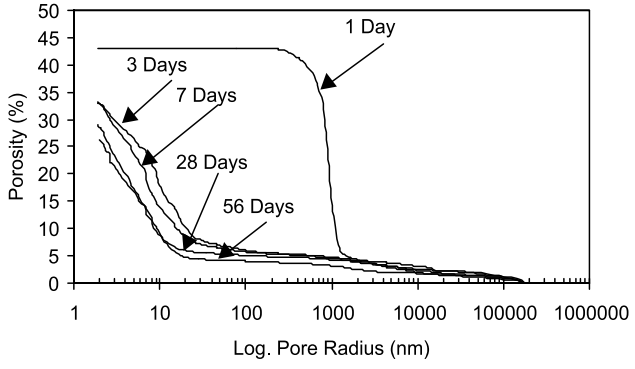

Fig. 4. Cumulative pore size distribution of bath cured AASP, $w/b = 0.5$.

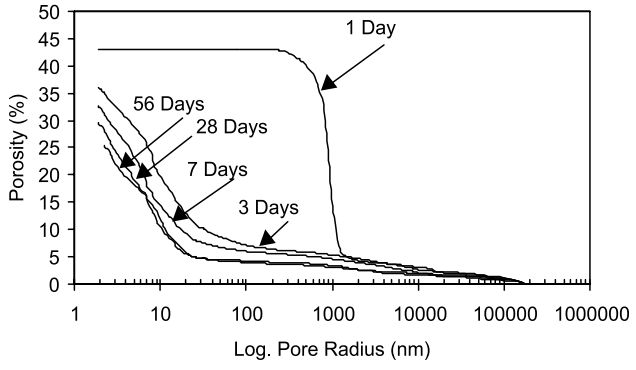

Fig. 5. Cumulative pore size distribution of sealed cured AASP, $w/b = 0.5$.

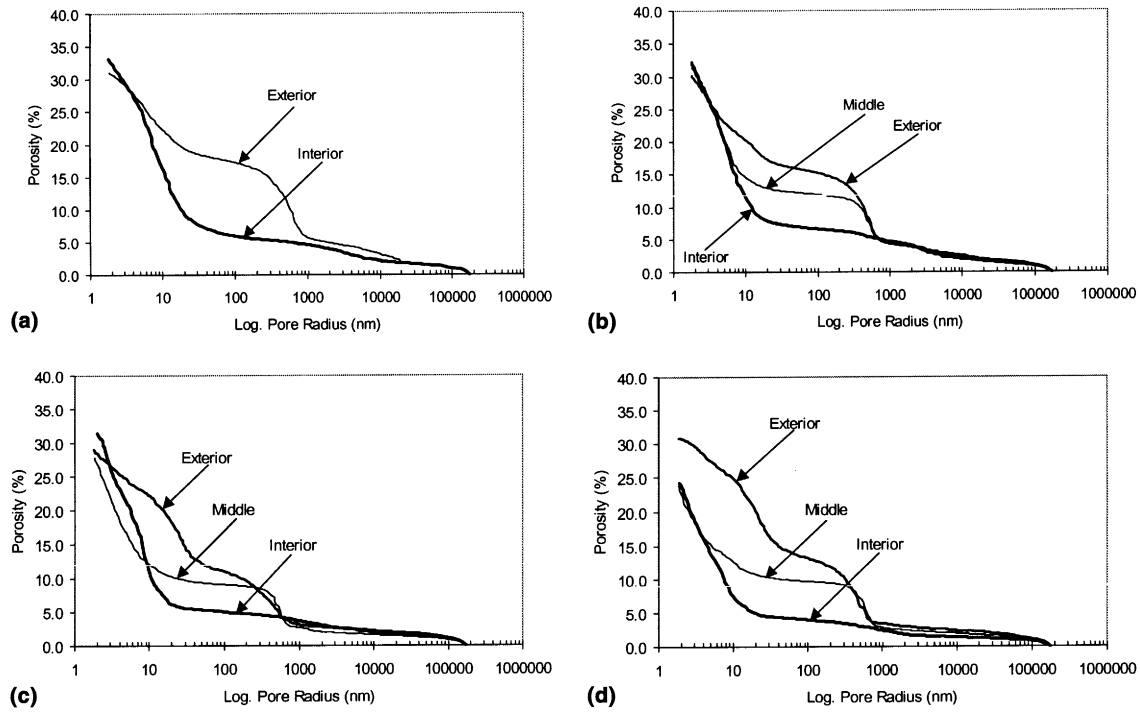

Fig. 6. Cumulative pore size distribution of exposed cured AASP, $w/b = 0.5$. (a) 3 days, (b) 7 days, (c) 28 days, (d) 56 days.

Table 3
Pore size proportions for AASP

Age (days)	% Mesopores (1.25–25 nm radius)	% Macropores (25–5000 nm radius)	% Voids/microcracks (5000–50,000 nm radius)
3	74.0	16.6	9.4
7	76.0	14.9	9.1
28	82.0	10.4	7.6
56	81.3	12.5	6.2

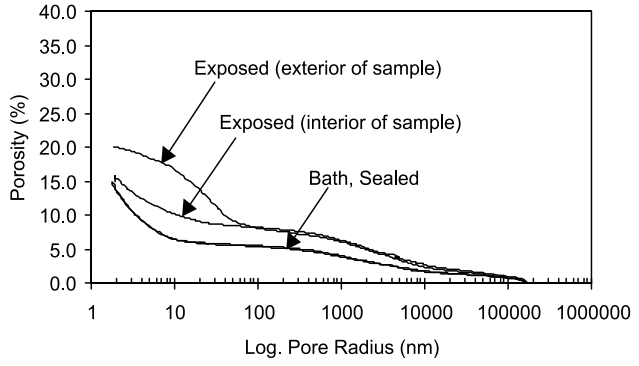

Fig. 7. Cumulative pore size distribution of bath, sealed, and exposed curing for 365 days.

6. Water sorptivity

Fig. 8 shows that following exposed curing AASC has increasing water sorptivity at ages beyond 3 days, indicating the existence of a network of interconnected microcracks within the sample that become progressively larger and continuous with increasing age. This indicates that the interconnected network of microcracks is a likely explanation for lower compressive strength of AASC following exposed curing.

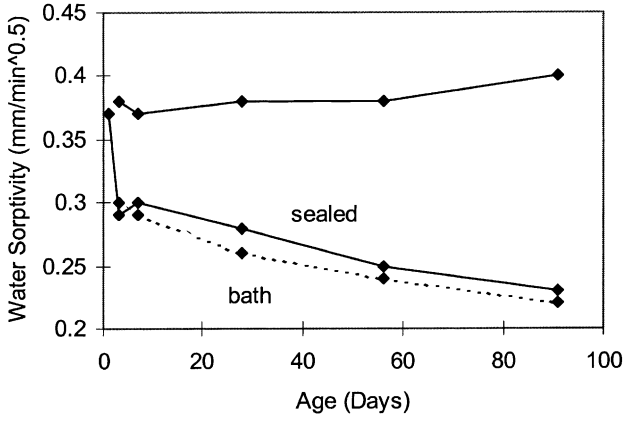

Fig. 8. Effect of curing on water sorptivity.

7. Conclusions

The compressive strength is almost identical when comparing bath cured AASC cylinders with sealed cured cylinders for $w/b = 0.5$. The laboratory exposed (23°C and 50% RH) cylinders have 41.4% and 53.5% lower compressive strength at 365 days than sealed and bath cured cylinders, respectively. Between 28 and 365 days the exposed cured cylinders show 17.2% strength loss.

Exposed AASC showed visible surface microcracks. The majority of microcracks occur within the first 3 days and are mostly of the size 0.01 mm. The frequency of the 0.01-mm crack size reaches a maximum at 7 days followed by crack width growth. The widths of microcracks are as high as 0.3 mm.

The effect of microcracking on exposed AASC samples were evident by considerably higher total porosity and coarser pore size distribution that was measured by MIPS testing.The pore size distribution of exposed AASP is more porous than bath and sealed samples, with the porosity increasing with distance towards the exterior of the sample. Following exposed curing, AASC shows that visible microcracking on the surface and water sorptivity testing showed the samples to have high uptake of water compared with bath and sealed cured companion cylinders. The high uptake of water can be associated with a continuous microcracking and capillary network, which has lead to inferior compressive strength. This shows that should AASC be used for construction it is imperative that the concrete is well cured.

Acknowledgements

The financial support for this project is jointly provided by Independent Cement and Lime Pty Ltd., Blue Circle Southern Cement Ltd. and Australian Steel Mill Services. The authors thank the sponsors, especially Alan Dow, Tom Wauer, Katherine Turner, Wayne James, Paul Ratcliff, John Ashby, and Dr. Ihor Hinczak for the guidance and support. The enthusiastic participation of final year student Dennis Kueh in this project is very much appreciated. The efforts and assistance with the laboratory work provided by Jeff Doddrell, Roger Doulis, and Peter Dunbar are also gratefully acknowledged.

References

[1] Anderson R, Gram H-E. Properties of alkali-activated slag. In: Anderson R, Gram H-E, Malolepszy J, Deja J, editors. Alkali-activated slag. Swedish Cement and Concrete Institute Report 1.88; 1988. p. 9–65.

[2] Bamforth PB, Pocock DC, Robery PC. The sorptivity of concrete. In: Proceedings of the International Conference on Our World in Concrete and Structures, Singapore, 1985 August 27–28. p. 1–33.

[3] Butler WB, Ashby JB. The influence of curing environment upon the properties of concrete made using a variety of Portland cement supplements. In: Proceedings of the Symposium of Technology of Concrete when Pozzolans, Slags, and Chemical Admixtures are used, Monterrey, Mexico, ACI-RILEM; 1985. p. 1–19.

[4] Butler WB, Ashby JB. A further report on the influence of curing environment upon the properties of concrete made using a variety of Portland cement supplements. Civil Engineering Transactions, Institution of Engineers. Australia; 1986. p. 45–55.

[5] Byfors K, Klingstedt G, Lehtonen V, Pyy H, Romben L. Durability of concrete made with alkali activated slag. In: Malhotra VM, editor. Proceedings of the Third International Conference on Fly Ash, Silica Fume, Slag, and Natural Pozzolans in Concrete, Trondheim, Norway, ACI SP 114-70; 1989. p. 1429–66.

[6] Carrasquillo RL, Slate FO, Nilson AH. Microcracking and behaviour of high strength concrete subject to short-term loading. ACI J 1981;78(3):179–86.

[7] Collins FG, Roper H. Evaluation of concrete spall repairs by pullout test. Mater Struct 1989;22:280–6.

[8] Collins FG, Sanjayan JG. Workability and mechanical properties of alkali activated slag concrete. Cem Conc Res 1998;29(3):455–8.

[9] Gjorv OE, Vennesland O. Diffusion of chloride ions from seawater into concrete. Cem Conc Res 1979;9(2):229–38.

[10] Hakkinen T, Pyy H, Koskinen P. Microstructural and permeability properties of alkali activated slag concrete. Technical Research Centre of Finland Research Report, 486; 1987. p. 1–69.

[11] Hakkinen T. The permeability of high strength blast furnace slag concrete. Nord Conc Res 1992;11:55–66.

[12] Hakkinen T. The microstructure of high strength blast furnace slag concrete. Nord Conc Res 1992;11:67–82.

[13] Hakkinen T. The influence of slag content on the microstructure, permeability and mechanical properties of concrete. Part 1. Cem Conc Res 1993;23(2):407–21.

[14] Hakkinen T. The influence of slag content on the microstructure, permeability and mechanical properties of concrete. Part 2. Technical properties and theoretical examinations. Cem Conc Res 1993;23(3):518–30.

[15] Hsu TTC, Slate FO, Sturman GM, Winter G. Microcracking of plain concrete and the shape of the stress-strain curve. J Am Conc Inst 1963;60:209–24.

[16] IUPAC. Manual of symbols and terminology. Appendix 2, Part 1, Colloid and surface chemistry. J Pure Appl Chem 1972;31:578.

[17] Kukko H, Mannonen R. Chemical and mechanical properties of alkali-activated blast furnace slag (F-concrete). Nord Conc Res 1982;1:16.1–16.16.

[18] Kutti T, Malinowski R. Influence of the curing conditions on the flexural strength of alkali activated blast furnace slag mortar. Nord Conc Res 1982;1:17.1–17.10.

[19] Kutti T, Berntsson L, Chandra S. Shrinkage of cements with high content of blast-furnace slag. In: Proceedings of the Fourth CANMET/ACI International Conference on Fly Ash, Silica Fume, Slag, and Natural Pozzolans in Concrete, Istanbul, Turkey, Supplementary Papers; 1992. p. 615–25.

[20] Li C, Yoda A, Yokomur T. Pore structure, strength and carbonation of cement pastes containing ground granulated blast-furnace slag. In: Malhotra VM, editor. Proceedings of the Sixth CANMET/ACI International Conference on Fly Ash, Silica Fume, Slag, and Natural Pozzolans in Concrete, Bangkok, Thailand, ACI SP 178; 1998. p. 875–91.

[21] Malolepszy J, Deja J. The influence of curing conditions on the mechanical properties of alkali activated slag binders. Silic Ind 1988;11–12:179–86.

[22] Manmohan D, Mehta PK. Influence of pozzolanic, slag, and chemical admixtures on pore size distribution and permeability of hardened cement pastes. Cem Conc Aggr 1981;3(1):63–7.
[23] Meyers BL, Slate FO, Winter G. Relationship between time-dependent deformation and microcracking of plain concrete. ACI J 1969;66(1):60–8.
[24] Nakamura N, Sakai M, Swamy RN. Effect of slag fineness on the engineering properties of high strength concrete. In: Swamy RN, editor. In: Proceedings of the International Conference on Blended Cements in Construction, University of Sheffield. Essex: Elsevier; 1991. p. 302–16.
[25] Ravindrarajah RS, Swamy RN. Load effects on fracture of concrete. Mater Struct 1989;22(127):15–22.
[26] Roy DM. Hydration, microstructure, and chloride diffusion of slag-cement pastes and mortars. In: Malhotra VM, editor. Proceedings of the Third International Conference on Fly Ash, Silica Fume, Slag, and Natural Pozzolans in Concrete, Trondheim, Norway, ACI SP-132, vol. 2; 1989. p. 1265–81.
[27] Roy DM, Idorn GM. Relation between strength, pore structure and associated properties of slagcontaining cementitious materials. In: Young JF, editor. Proceedings of the Materials Research Symposium on Very High Strength CementBased Materials, Boston, Massachusetts, USA, vol. 42; 1985. p. 133–42.
[28] Roy DM, Silsbee MR. Overview of slag microstructure and alkali activated slag in concrete. In: Proceedings of the Second CANMET/ACI International Symposium on Advances in Concrete Technology, Las Vegas, USA, Supplementary Papers; 1995. p. 699–716.
[29] Sicard V, Francois R, Ringot E, Pons G. Influence of creep and shrinkage on cracking in high strength concrete. Cem Conc Res 1992;22(1):159–68.
[30] Sioulas B. In situ strength and temperature characteristics of high strength concrete incorporating slag. Masters thesis. Department of Civil Engineering, Monash University, Clayton, Australia; 1996.
[31] Swamy RN, Bouikni A. Some engineering properties of slag concrete as influenced by mix proportioning and curing. ACI Mater J 1990;87(3):210–20.
[32] Talling B. Effect of curing conditions on alkali-activated slags. In: Malhotra VM, editor. Proceedings of the Third International Conference on Fly Ash, Silica Fume, Slag, and Natural Pozzolans in Concrete, Trondheim, Norway, ACI SP-114, vol. 2; 1989. p. 1485–500.
[33] Talling B, Brandstetr J. Present state and future of alkali-activated slag concretes. In: Malhotra VM, editor. Proceedings of the Third International Conference on Fly Ash, Silica Fume, Slag, and Natural Pozzolans in Concrete, Trondheim, Norway, ACI SP 114, vol. 2; 1989. p. 1519–46.
[34] Wainwright PJ. Properties of fresh and hardened concrete incorporating slag cement. In: Swamy RN, editor. Concrete technology and design, cement replacement materials, vol. 3. Bishopbriggs, Glasgow: Surrey University Press; 1986. p. 100–33.
[35] Wainwright PJ, Reeves CM. Properties of slag concrete: UK experience. In: Ryan WG, editor. Proceedings of the Concrete Workshop 88, International Workshop on the use of Fly Ash, Slag, Silica Fume and Other Siliceous Materials in Concrete, Sydney, Australia, July 4–6 1988. p. 168–98.